

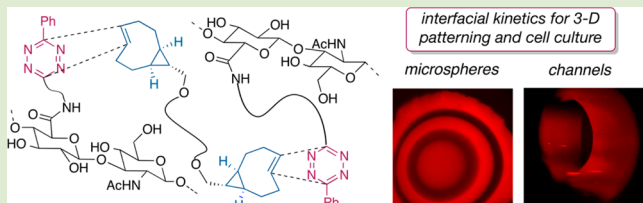
## Interfacial Bioorthogonal Cross-Linking

Han Zhang,<sup>†</sup> Kevin T. Dicker,<sup>†</sup> Xian Xu, Xinqiao Jia,\* and Joseph M. Fox\*

Departments of Chemistry and Biochemistry and Materials Science and Engineering, University of Delaware, Newark, Delaware 19716, United States

### Supporting Information

**ABSTRACT:** Described herein is interfacial bioorthogonal cross-linking, the use of bioorthogonal chemistry to create and pattern biomaterials through diffusion-controlled gelation at the liquid-gel interface. The basis is a rapid ( $k_2$  284000 M<sup>-1</sup> s<sup>-1</sup>) reaction between strained *trans*-cyclooctene (TCO) and tetrazine (Tz) derivatives. Syringe delivery of Tz-functionalized hyaluronic acid (HA-Tz) to a bath of bis-TCO cross-linker instantly creates microspheres with a cross-linked shell through which bis-TCO diffuses freely to introduce further cross-linking at the interface. Tags can be introduced with 3D resolution without external triggers or templates. Water-filled hydrogel channels were prepared by simply reversing the order of addition. Prostate cancer cells encapsulated in the microspheres have 99% viability, proliferate readily, and form aggregated clusters. This process is projected to be useful in the fabrication of cell-instructive matrices for in vitro tissue models.



The construction of cell-instructive hydrogel networks represents the first step toward in vitro engineering of functional tissues.<sup>1,2</sup> For tissue engineering, it is essential that synthetic matrices mimic the natural extracellular matrix by presenting molecular cues in a spatially defined manner without adversely affecting living cells. While various modes of reactivity have been explored for the hydrogel synthesis, efficient network formation at well-defined interfaces with close to 100% overall cell viability has not yet been reported.

Bioorthogonal reactions<sup>3–5</sup> have emerged as important tools for tissue engineering.<sup>6–9</sup> In 2008, rapid bioorthogonal reactions of *s*-tetrazine (Tz) and *trans*-cyclooctene (TCO)<sup>10</sup> or norbornene<sup>11</sup> derivatives were described.<sup>10,12–14</sup> With our recent TCO derivatives,<sup>15</sup> rate constants of  $k_2 > 10^5$  M<sup>-1</sup> s<sup>-1</sup> have been measured.<sup>16,17</sup> Tetrazine-norbornene chemistry has been applied to polymer synthesis and hydrogel fabrication.<sup>18–20</sup> Separately, TCO-modified polymers have been used for radiochemistry and TCO has been used in nanoparticle bioconjugation.<sup>21,22</sup> However, TCO-tetrazine ligation has not been used for cross-linking or polymerization purposes.

Here, we demonstrate the use of bioorthogonal chemistry to create covalently cross-linked hydrogel materials through a rapid reaction at the gel–liquid interface (Figure 1a). Interfacial reactions are extensively utilized in polymer science, with the interfacial polymerization of nylon serving as the archetypical example.<sup>23</sup> Anseth and Bowman have elegantly shown that enzyme-mediated interfacial radical chain polymerization can be used to create multilayered hydrogels.<sup>24</sup> Interfacial cross-linking processes have also been used for cell encapsulation purposes, most typically employing the anionic polysaccharide alginic acid.<sup>25</sup> While alginate microspheres meet many of the requirements for the immunoisolation of cells, they lack in vivo

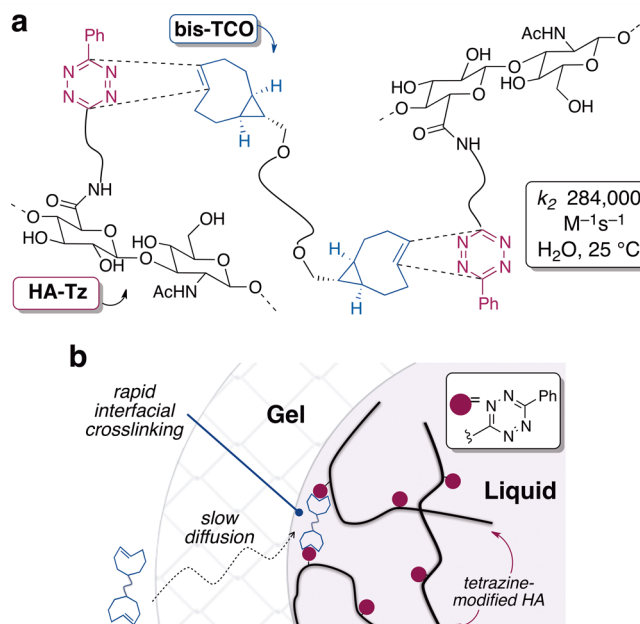


**Figure 1.** (a) Instantaneous cross-linking via tetrazine-TCO ligation. (b) Gel interface forms when a droplet of tetrazine-modified hyaluronic (HA-Tz) contacts a solution of bis-*trans*-cyclooctene cross-linker (bis-TCO). Cross-linking at the gel/liquid interface is faster than the rate of diffusion through the gel interface.

stability and mechanical strength, due to weakening of the hydrogel core by ex-change of calcium.<sup>26</sup>

Received: May 16, 2014

Accepted: June 28, 2014

Published: July 14, 2014

This report describes the first interfacial process based on a bioorthogonal reaction.<sup>24,27</sup> The building block chosen for study was hyaluronic acid (HA), a natural polysaccharide previously used to create hydrogels for drug delivery and tissue engineering.<sup>28–30</sup> Recently, furan/maleimide chemistry has been used to create HA-based hydrogels that can be subsequently photopatterned with biomolecules using two-photon laser processing.<sup>31</sup> Distinguishing features of the approach described here are the interfacial kinetics and bioorthogonality of the inverse electron demand Diels–Alder reaction with TCO. Diffusion controlled bioorthogonal cross-linking also differs from previously described methods for the self-assembly of HA at the aqueous liquid–liquid interface<sup>27</sup> and complements methods for 3D patterning of biomolecules based on photochemistry.<sup>32</sup>

The building blocks for interfacial cross-linking could be constructed from precursors that were readily available on multigram scale. Shown in Figure 2 are tetrazine-modified HA

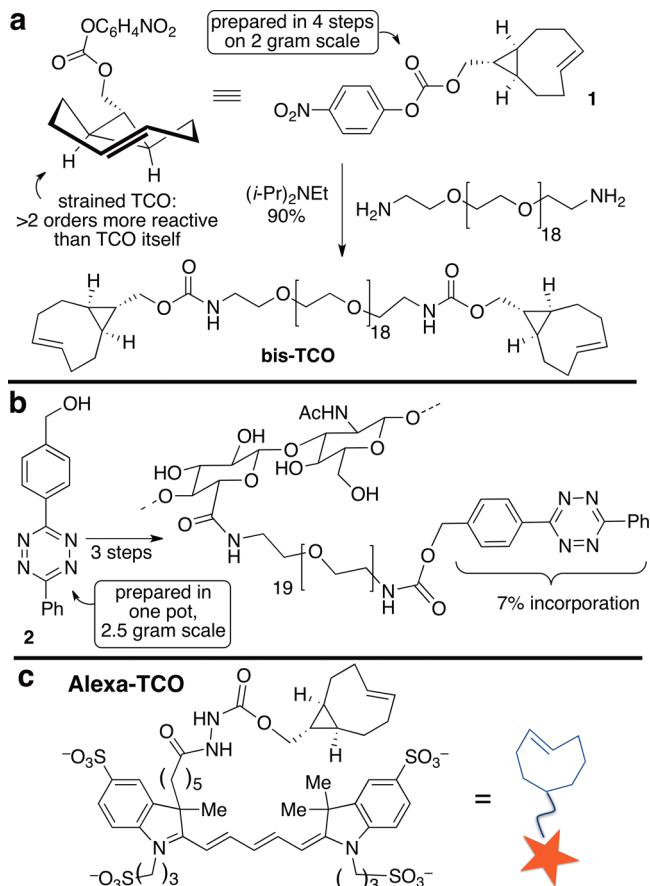


**Figure 2.** Synthesis of (a) bis-TCO, (b) HA-Tz, and (c) chemical structure of Alexa-TCO conjugate. The level of tetrazine incorporation (7%) was chosen in order to target the desired gel stiffness for the 3D culture of LNCaP prostate cancer cells.

(HA-Tz) and a cross-linker (bis-TCO). The cross-linker was prepared from a computationally designed TCO with exceptional reactivity due to conformational strain<sup>15</sup> (Figure 2). In water at 25 °C,  $k_2$  284000 ( $\pm$ 13000) M<sup>-1</sup> s<sup>-1</sup> was measured for a model reaction by stopped-flow analysis.

An interfacial cross-linking protocol for the synthesis of HA hydrogel microspheres was devised (Figures 1b and 3a). Disappearance of the pink tetrazine chromophore upon

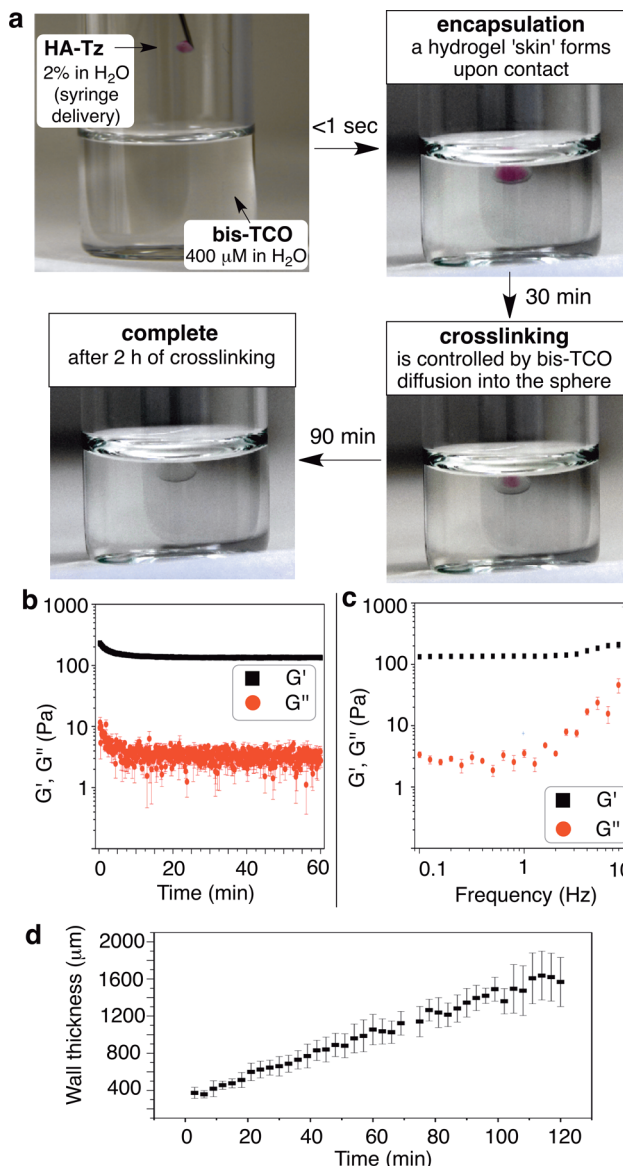


**Figure 3.** (a) Microsphere forms a hydrogel “skin” on contact of HA-Tz droplet with a bis-TCO cross-linker bath. Cross-linking is diffusion controlled. (b, c) Rheological properties of interfacially cross-linked HA microspheres:  $G'$ , elastic modulus;  $G''$ , loss modulus. (d) The cross-linked wall thickness of the microsphere as a function of diffusion time.

reaction allowed visual monitoring. Microspheres were prepared by adding droplets of an HA-Tz solution (2 wt %) to bis-TCO (400  $\mu$ M). A cross-linked shell forms on contact, as evidenced by a colorless layer around the pink core (Figure 3a). Subsequent cross-linking is controlled by diffusion resulting in the inward advancement of a distinct gel/liquid interface. The bis-TCO cross-linker (MW 1253) diffuses across the gel layer readily, but HA-Tz ( $M_v$  218 kDa) cannot. Thus, cross-linking takes place at the inner gel/liquid interface of the microsphere, with the volume of the pink, un-cross-linked HA-Tz core steadily decreasing as the wall thickness increases. The microsphere was fully swollen after the synthesis (equilibrium swelling ratio 49  $\pm$  2). Oscillatory rheometry was performed on as-synthesized microspheres by sandwiching the sample between the parallel plate geometry. Time sweep experiments (Figure 3b) show a stable plateau  $G'$  value of 135  $\pm$  5 Pa (with

$G'' < 10 \text{ Pa}$ ) after the initial decrease during the first 2–3 min, due possibly to compression-induced network stiffening,<sup>33</sup> followed by network relaxation. The insensitivity of  $G'$  (Figure 3c) to frequency is consistent with an elastic, covalently cross-linked gel. As shown in Figure 3d, the wall thickness increases linearly as a function of diffusion time over 2 h (Figure 3d).

Diffusion-controlled cross-linking also presented a way to functionalize microspheres with spatial resolution. We reasoned that diffusible TCO conjugates could be covalently introduced at the interface, and that the thickness of the resulting “tagged” gel layer would be a function of cross-linking time. Subsequent exchange with a label-free solution of bis-TCO would result in gels with distinct tagged and blank layers (Figure 4a). Thus, a droplet of HA-Tz (2 wt %) was added to bis-TCO (400  $\mu\text{M}$ ) containing Alexa-TCO (1  $\mu\text{M}$ ), a fluorescent conjugate (structure in Figure 2c). After 30 min, the bath was replaced by dye-free bis-TCO (400  $\mu\text{M}$ ), and cross-linking continued for 2 h. Confocal microscopy showed microspheres with an  $\sim 400 \mu\text{m}$  thick fluorescent shell (Figure 4b). Separately, a droplet was initially exposed to dye-free bis-TCO (60 min) prior to adding Alexa-TCO (1  $\mu\text{M}$ ), giving core-labeled microspheres (1.45 mm diameter) with a shell (900  $\mu\text{m}$ ) that was only faintly stained (Figure 4c). Multilayer structures were created by simply alternating the presence/absence of Alexa-TCO during cross-linking. Figure 4d–f shows HA microspheres containing 3, 5, and 7 distinct layers.<sup>34</sup>

Microspheres with radial gradients of fluorescent tags were readily created by syringe pump introduction of Alexa-TCO during cross-linking. The concentration of Alexa-TCO was nil when the shell of the microsphere was cross-linked, and the concentration of the fluorescent tag was gradually increased as interfacial cross-linking proceeded toward the center of microsphere, with an Alexa-TCO concentration of 0.47  $\mu\text{M}$  when the core of the microsphere was cross-linked. As shown by the confocal image of the central slice of the z-stack in Figure 4g with the accompanying color intensity plot in Figure 4h, this protocol produced microspheres with distinct radial gradients where fluorescence intensity is highest at the core. This gradient technique holds promise for creating cell culture matrices that can recapitulate the ligand density and clustering effects important in cell adhesion and signaling.

Of note, these gradient and layered structures can be prepared without external triggers<sup>35,36</sup> or pre-existing templates,<sup>37,38</sup> and two independent chemistries for cross-linking and patterning purposes are not required.<sup>8,39</sup> With these tools, we envision use of bioorthogonal cross-linking for 3D covalent patterning of cell-instructive molecules that modulate cell adhesion, signaling and differentiation.

Interfacial bioorthogonal cross-linking also enables the preparation of water-filled hydrogel channels (Figure 5). When a bis-TCO solution (2 mM) was introduced to HA-Tz (2 wt %) via syringe, a cross-linked wall instantly followed the path of the needle (Movie S1). During interfacial cross-linking, HA-Tz was simultaneously tagged by Alexa-TCO, which was added for visualization (Figure 5b–d). After 1 min, the channel wall thickness was  $155 \pm 13 \mu\text{m}$  and free Alexa-TCO remained in the interior (Figure 5b). After 15 min, the wall was  $254 \pm 18 \mu\text{m}$  thick and the fluorescence inside the channel decreased (Figure 5e). We reason that bis-TCO and Alexa-TCO exhibit a similar rate of diffusion across the cross-linked shell, whereas HA-Tz in the reservoir is excluded from penetrating into the channel due to its large size. Thus, the cross-linking front extends outward and generates water-filled channels. The wall

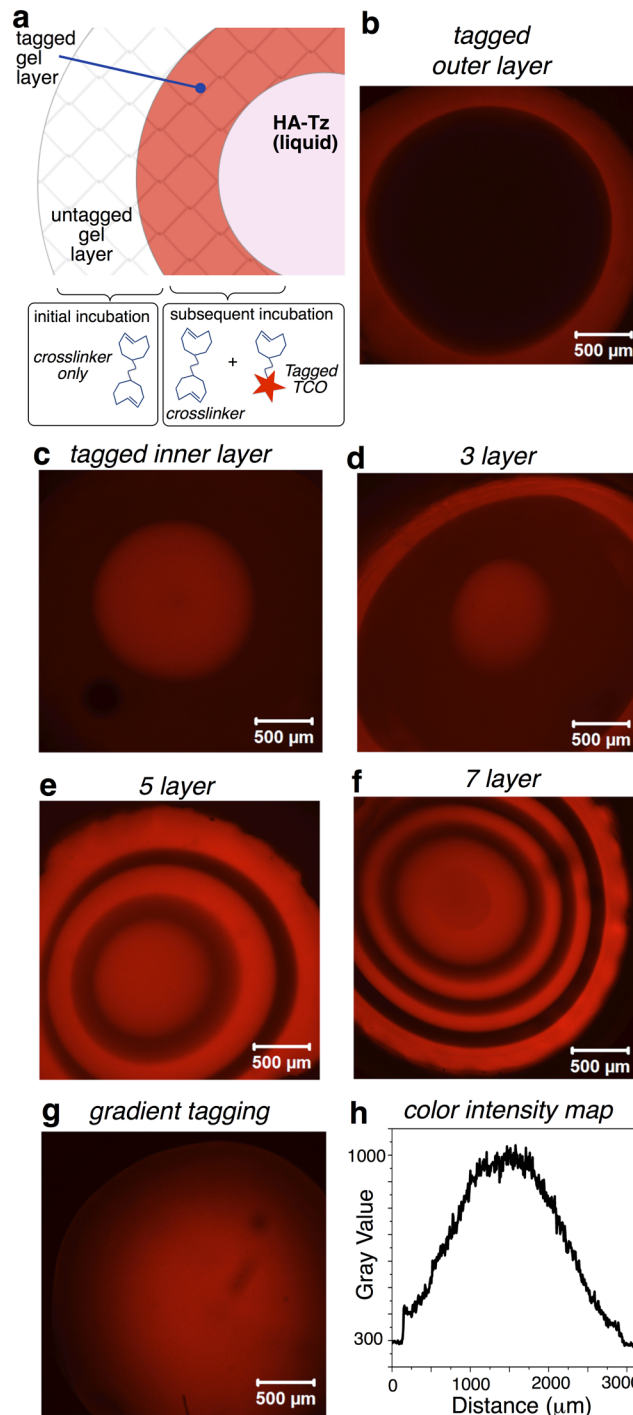


**Figure 4.** (a) Interfacial covalent tagging; (b–g) Confocal microscopy images and (h) image intensity plot. (b) Interfacial cross-linking initially in the presence (30 min) then absence (90 min) of Alexa-TCO gave shell-labeled microspheres. (c) Cross-linking in the absence (60 min) and then presence (60 min) of Alexa-TCO gave core-labeled microspheres. (d–f) Onion-like structures by alternating the presence and absence of Alexa-TCO during the cross-linking procedure: three-, five-, and seven-layered gels are displayed. (g) Radial gradients were produced by increasing the concentration of Alexa-TCO (0.47  $\mu\text{M}$ ) during the 120 min of cross-linking and confirmed by (h) measuring the color intensity across the diameter of the central slice of the microsphere.

thickness at 30 and 60 min was  $262 \pm 18 \mu\text{m}$  with no significant increase thereafter. These observations on wall

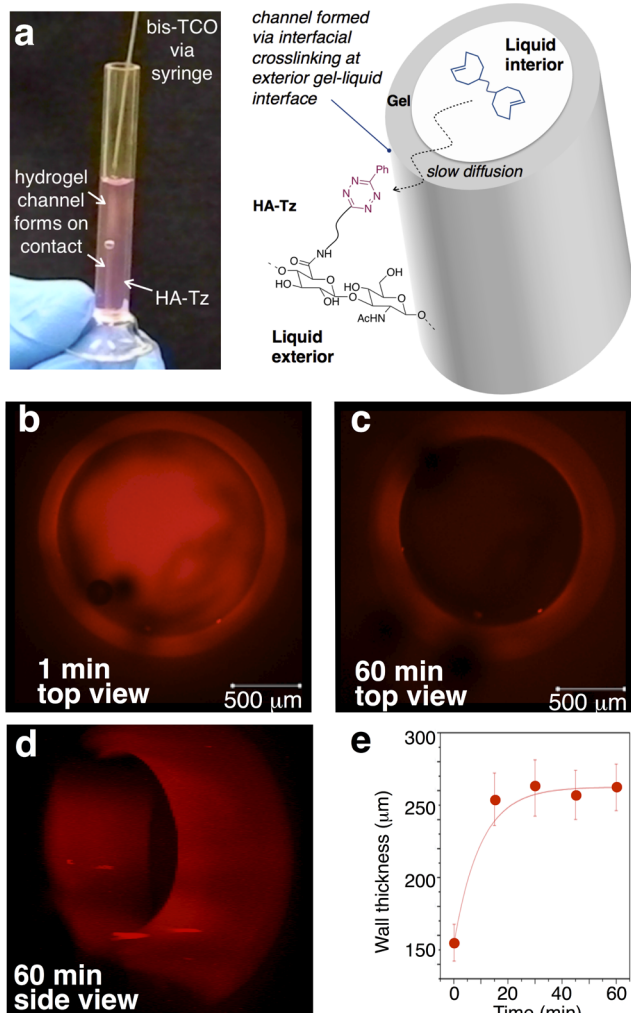


**Figure 5.** (a) Bis-TCO is drawn through a solution of HA-Tz, creating a water-filled channel. Bis-TCO diffuses outward, increasing the wall thickness via cross-linking at the outer interface. (b–d) Hydrogel channel pulled by injecting bis-TCO (2 mM)/Alexa-TCO (2  $\mu$ M) into a solution of HA-Tz (2 wt %). z-Stack confocal images show the following: (a) 1 min, walls ( $153 \pm 13 \mu\text{m}$ ) with unreacted dye in the interior; (c, d) 60 min, dye almost completely migrated out of the lumen. (e) Plot of channel wall thickness as a function of diffusion time.

thickness are consistent with a limiting amount of the bis-TCO cross-linker within the lumen of the channel, as the wall ceased to thicken when the cross-linker was depleted. The projected confocal images (Figure 5 and Movies S2–S3) convincingly show the creation of a hollow channel by this simple injection process without the need to use pre-existing templates.<sup>40</sup>

We next investigated if interfacial cross-linking could be applied to engineer a physiologically relevant *in vitro* tumor model. Such *in vitro* models are critically needed for drug testing and discovery, as many cancer cell lines (e.g., prostate cancer<sup>41</sup>) cultured in 2D exhibit nonphysiological morphology and drug response.<sup>42</sup> As shown in Figure 6, prostate cancer LNCaP cells suspended in HA-Tz could indeed be encapsulated in microspheres. The level of tetrazine incorporation (7%) was selected to give soft, elastic gels appropriate for the 3D culture of LNCaP prostate cancer cells.<sup>43,44</sup> Live/dead staining (Figure S7) revealed 99 and 98% cell viability at days 1 and 5, respectively, confirming the cytocompatibility of tetrazine

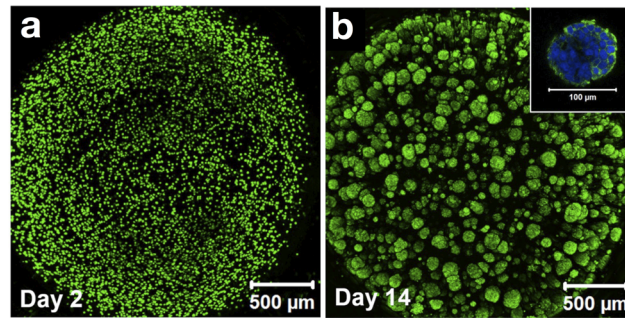


**Figure 6.** Bioorthogonal cross-linking is cytocompatible to LNCaP cells. Confocal images after live/dead staining showing (a) individually dispersed LNCaP cells at day 2 and (b) dispersed tumoroids at day 14. The inset shows an  $\sim 100 \mu\text{m}$  aggregate strained for F-actin (green) and nuclei (blue) at day 14. (c) Cell proliferation assay (Trypan Blue exclusion),  $*p < 0.05$ .

ligation. LNCaP cells initially entrapped homogeneously in a single cell state proliferated readily (Figure 6) and neighboring cell clusters merged within the microsphere. Cells in individual aggregates displayed rounded, clustered morphology with apparent cortical organization of actin.<sup>43</sup> Individual microspheres were completely populated by over 200 dispersed tumor aggregates each greater than  $50 \mu\text{m}$ .

In summary, interfacial bioorthogonal cross-linking has been developed and applied to the construction of hydrogel channels and microspheres. These materials can be covalently tagged with 3D resolution and utilized as matrices for cell culture. We project continued utility of this process to the fabrication and molecular patterning of cell-instructive matrices for *in vitro* tissue culture.

## ASSOCIATED CONTENT

### S Supporting Information

Experimental procedures, NMR spectra, movies of hydrogel channels, stopped-flow data, cell viability data, viscosity data, and microsphere color intensity maps. This material is available free of charge via the Internet at <http://pubs.acs.org>.

## AUTHOR INFORMATION

### Corresponding Authors

\*E-mail: jmfox@udel.edu.  
\*E-mail: xjia@udel.edu.

### Author Contributions

<sup>†</sup>These authors contributed equally (H.Z. and K.T.D.).

### Notes

The authors declare no competing financial interest.

## ACKNOWLEDGMENTS

We thank J. Caplan and Z. Tong for confocal imaging assistance and Genzyme for providing HA. We thank NSF

(DMR1206310) and NIH (NIDCR, R01 DE022969) for financial support. For instrumentation, we thank NSF CHE0840401, NSF CHE1229234, NIH S10 RR026962, COBRE 2P20RR017716. K.T.D. thanks R. W. Gore Fellowship Program.

## ■ REFERENCES

- (1) Lutolf, M. P.; Gilbert, P. M.; Blau, H. M. *Nature* **2009**, *462* (7272), 433–441.
- (2) Huebsch, N.; Mooney, D. J. *Nature* **2009**, *462* (7272), 426–432.
- (3) Kolb, H. C.; Finn, M. G.; Sharpless, K. B. *Angew. Chem., Int. Ed.* **2001**, *40* (11), 2004–2021.
- (4) Patterson, D. M.; Nazarova, L. A.; Prescher, J. A. *ACS Chem. Biol.* **2014**, *9* (3), 592–605.
- (5) Sletten, E. M.; Bertozzi, C. R. *Angew. Chem., Int. Ed.* **2009**, *48* (38), 6974–6998.
- (6) Hawker, C. J.; Wooley, K. L. *Science* **2005**, *309* (5738), 1200–1205.
- (7) Agard, N. J.; Prescher, J. A.; Bertozzi, C. R. *J. Am. Chem. Soc.* **2004**, *126* (46), 15046–15047.
- (8) DeForest, C. A.; Anseth, K. S. *Nat. Chem.* **2011**, *3* (12), 925–931.
- (9) Jiang, Y.; Chen, J.; Deng, C.; Suuronen, E. J.; Zhong, Z. *Biomaterials* **2014**, *35* (18), 4969–4985.
- (10) Blackman, M. L.; Royzen, M.; Fox, J. M. *J. Am. Chem. Soc.* **2008**, *130* (41), 13518–13519.
- (11) Devaraj, N. K.; Weissleder, R.; Hilderbrand, S. A. *Bioconjugate Chem.* **2008**, *19* (12), 2297–2299.
- (12) Selvaraj, R.; Fox, J. M. *Curr. Opin. Chem. Biol.* **2013**, *17*, 753–760.
- (13) Devaraj, N. K.; Weissleder, R. *Acc. Chem. Res.* **2011**, *44* (9), 816–827.
- (14) Ščekutė, J.; Devaraj, N. K. *Curr. Opin. Chem. Biol.* **2013**, *17* (5), 761–767.
- (15) Taylor, M. T.; Blackman, M. L.; Dmitrenko, O.; Fox, J. M. *J. Am. Chem. Soc.* **2011**, *133* (25), 9646–9649.
- (16) Rossin, R.; van den Bosch, S. M.; ten Hoeve, W.; Carvelli, M.; Versteegen, R. M.; Lub, J.; Robillard, M. S. *Bioconjugate Chem.* **2013**, *24* (7), 1210–1217.
- (17) Lang, K.; Davis, L.; Wallace, S.; Mahesh, M.; Cox, D. J.; Blackman, M. L.; Fox, J. M.; Chin, J. W. *J. Am. Chem. Soc.* **2012**, *134* (25), 10317–10320.
- (18) Hansell, C. F.; Espeel, P.; Stamenovic, M. M.; Barker, I. A.; Dove, A. P.; Du Prez, F. E.; O'Reilly, R. K. *J. Am. Chem. Soc.* **2011**, *133* (35), 13828–13831.
- (19) Cok, A. M.; Zhou, H.; Johnson, J. A. *Macromol. Symp.* **2013**, *329* (1), 108–112.
- (20) Alge, D. L.; Azagarsamy, M. A.; Donohue, D. F.; Anseth, K. S. *Biomacromolecules* **2013**, *14* (4), 949–953.
- (21) Haun, J. B.; Devaraj, N. K.; Hilderbrand, S. A.; Lee, H.; Weissleder, R. *Nat. Nanotechnol.* **2010**, *5* (9), 660–665.
- (22) Kelihier, E. J.; Reiner, T.; Turetsky, A.; Hilderbrand, S. A.; Weissleder, R. *ChemMedChem* **2011**, *6* (3), 424–427.
- (23) Odian, G. *Principles of Polymerization*, 4th ed.; John Wiley & Sons, Inc.: Hoboken, NJ, 2004.
- (24) Johnson, L. M.; DeForest, C. A.; Pendurthi, A.; Anseth, K. S.; Bowman, C. N. *ACS Appl. Mater. Interfaces* **2010**, *2* (7), 1963–1972.
- (25) Lim, F.; Sun, A. M. *Science* **1980**, *210* (4472), 908–910.
- (26) Dumitriu, S.; Popa, V. *Polymeric Biomaterials: Structure and Function*; CRC Press: Boca Raton, FL, 2013; Vol. 1, pp 280–281.
- (27) Capito, R. M.; Azevedo, H. S.; Velichko, Y. S.; Mata, A.; Stupp, S. I. *Science* **2008**, *319* (5871), 1812–1816.
- (28) Garg, H. G.; Hales, C. A. *Chemistry and Biology of Hyaluronan*, 1st ed.; Elsevier Ltd.: Oxford, 2004.
- (29) Burdick, J. A.; Prestwich, G. D. *Adv. Mater.* **2011**, *23* (12), H41–H56.
- (30) Xu, X.; Jha, A. K.; Harrington, D. A.; Farach-Carson, M. C.; Jia, X. *Soft Matter* **2012**, *8* (12), 3280–3294.
- (31) Owen, S. C.; Fisher, S. A.; Tam, R. Y.; Nimmo, C. M.; Shoichet, M. S. *Langmuir* **2013**, *29* (24), 7393–7400.
- (32) Torgersen, J.; Qin, X. H.; Li, Z. Q.; Ovsianikov, A.; Liska, R.; Stampfl, J. *Adv. Funct. Mater.* **2013**, *23* (36), 4542–4554.
- (33) Erk, K. A.; Henderson, K. J.; Shull, K. R. *Biomacromolecules* **2010**, *11* (5), 1358–1363.
- (34) Displayed in the Supporting Information are color intensity plots that accompany Figure 4b–f and a control experiment where Alexa-TCO concentration was held constant.
- (35) Bajaj, P.; Marchwiany, D.; Duarte, C.; Bashir, R. *Adv. Healthcare Mater.* **2013**, *2* (3), 450–458.
- (36) Luo, Y.; Shoichet, M. S. *Nat. Mater.* **2004**, *3* (4), 249–253.
- (37) Lee, W.; Park, J. *Adv. Mater.* **2012**, *24* (39), 5339–5344.
- (38) Occhetta, P.; Sadr, N.; Piraino, F.; Redaelli, A.; Moretti, M.; Rasponi, M. *Biofabrication* **2013**, *5* (3), 035002.
- (39) Khetan, S.; Burdick, J. A. *Soft Matter* **2011**, *7* (3), 830–838.
- (40) Miller, J. S.; Stevens, K. R.; Yang, M. T.; Baker, B. M.; Nguyen, D. H. T.; Cohen, D. M.; Toro, E.; Chen, A. A.; Galie, P. A.; Yu, X.; Chaturvedi, R.; Bhatia, S. N.; Chen, C. S. *Nat. Mater.* **2012**, *11* (9), 768–774.
- (41) Hutmacher, D. W.; Loessner, D.; Rizzi, S.; Kaplan, D. L.; Mooney, D. J.; Clements, J. A. *Trends Biotechnol.* **2010**, *28* (3), 125–133.
- (42) Goodman, T. T.; Ng, C. P.; Pun, S. H. *Bioconjugate Chem.* **2008**, *19* (10), 1951–1959.
- (43) Xu, X.; Gurski, L. A.; Zhang, C.; Harrington, D. A.; Farach-Carson, M. C.; Jia, X. Q. *Biomaterials* **2012**, *33* (35), 9049–9060.
- (44) Xu, X.; Sabanayagam, C. R.; Harrington, D. A.; Farach-Carson, M. C.; Jia, X. *Biomaterials* **2014**, *35* (10), 3319–3330.